Acta Crystallographica Section D
Biological Crystallography
ISSN 0907-4449

REACH: Robotic Equipment for Automated Crystal Harvesting using a six-axis robot arm and a micro-gripper

Mohammad Yaser Heidari Khajepour,[a] Xavier Vernede,[a,b] David Cobessi,[a] Hugo Lebrette,[b] Pierrick Rogues,[c] Maxime Terrien,[a] Christophe Berzin[a] and Jean-Luc Ferrer[a]*

[a]Institut de Biologie Structurale Jean-Pierre Ebel, Groupe Synchrotron, Commissariat à l'Energie Atomique et aux Energies Alternatives, Centre National de la Recherche Scientifique, Université Joseph Fourier, F-38027 Grenoble CEDEX 1, France, [b]Institut de Biologie Structurale Jean-Pierre Ebel, Groupe MetalloProtéines, Commissariat à l'Energie Atomique et aux Energies Alternatives, Centre National de la Recherche Scientifique, Université Joseph Fourier, F-38027 Grenoble CEDEX 1, France, and [c]NatX-ray, 38400 Saint Martin d'Hères, France

Correspondence e-mail: jean-luc.ferrer@ibs.fr

Received 30 June 2012
Accepted 21 November 2012

In protein crystallography experiments, only two critical steps remain manual: the transfer of crystals from their original crystallization drop into the cryoprotection solution followed by flash-cooling. These steps are risky and tedious, requiring a high degree of manual dexterity. These limiting steps are a real bottleneck to high-throughput crystallography and limit the remote use of protein crystallography core facilities. To eliminate this limit, the Robotic Equipment for Automated Crystal Harvesting (REACH) was developed. This robotized system, equipped with a two-finger micro-gripping device, allows crystal harvesting, cryoprotection and flash-cooling. Using this setup, harvesting experiments were performed on several crystals, followed by direct data collection using the same robot arm as a goniometer. Analysis of the diffraction data demonstrates that REACH is highly reliable and efficient and does not alter crystallographic data. This new instrument fills the gap in the high-throughput crystallographic pipeline.

1. Introduction

Protein structure determination by X-ray crystallography involves numerous steps. In recent years, most of these steps, such as protein purification (Kim *et al.*, 2004), crystallization (Mueller-Dieckmann, 2006) and data collection and processing, have been mostly automated (Adams *et al.*, 2011; Ferrer, 2001; Manjasetty *et al.*, 2008). The critical steps that remain are harvesting crystals from their crystallization drop for crystals grown using the vapour-diffusion method (McPherson, 1989), followed by cryoprotection and flash-cooling. These steps are still managed manually. Owing to their high solvent content, protein crystals are very fragile and may easily be damaged by variation of temperature and ambient humidity or mechanical stress. As a consequence, manual harvesting, which is sometimes made even more difficult by the small dimensions of protein crystals (from ∼10 to ∼500 µm), can easily induce damage. This is further aggravated by the high-throughput 'nanodrop' crystallization robots that are mostly used nowadays, where even smaller crystals are grown in the range from ∼5 to ∼50 µm. *In situ* diffraction in the crystallization drop at room temperature is an alternative to crystal harvesting (Jacquamet *et al.*, 2004). Nevertheless, because of limitations owing to crystal symmetry and crystal degradation during beam exposure at room temperature, harvesting and flash-cooling of samples are very often necessary.

Over the past few decades, the most common method of harvesting protein crystals has been to use microloops (Teng, 1990). Crystals are visualized through a binocular microscope and manipulated manually in their crystallization drops. First of all, harvesting crystals in this configuration is very annoying as the microscope blocks easy access to the drop. If the crystals

are obtained using the hanging-drop technique, access to the drop is a little easier. However, in high-throughput protein crystallization setups crystals are usually produced in microlitre to nanolitre sitting drops dispensed with pipetting robots onto 96-well microplates. Manipulation of crystals into these drops requires more dexterity owing to the geometry of the microplates. Furthermore, since the volume of the crystallization drops is reduced, rapid manipulation is required to avoid evaporation. Secondly, manipulating crystals requires a high degree of delicacy and dexterity. Crystals may sometimes be trapped in a skin at the surface of the drop or may be stuck to the bottom of the well. In these difficult situations, performing harvesting manually stresses the crystal and could harm or even destroy it. Thirdly, in most cases, once the crystal is harvested on a loop it has to be transferred into a cryoprotecting solution before flash-cooling (Parkin & Hope, 1998). Consequently, in most cases, the crystal will be released into the cryoprotecting drop and has to be harvested once again. Finally, crystals should be flash-cooled to avoid the formation of ice (Kriminski *et al.*, 2002) and will need to be kept at a temperature below 140 K (Garman & Schneider, 1997). The most traditional methods are to plunge the loop into liquid nitrogen (77 K) or to expose the loop to a 100 K nitrogen-gas stream. The reproducibility of these operations is quite random as they are managed manually (Warkentin *et al.*, 2006).

At least five different robotic harvesting systems for protein crystals have been developed in the last decade: one with a two-finger manipulator system (Ohara *et al.*, 2004); another with a traditional harvesting loop on a six-axis robot arm (Viola *et al.*, 2011); the 'Crystal Harvester' with two motorized loops (Bruker AXS); a system that uses a series of micromanipulators for seeding and harvesting protein crystals (Georgiev *et al.*, 2004, 2006); and a recently developed system that cuts off the sealing tape and collects the entire drop hanging on it (Cipriani *et al.*, 2012). In spite of their numerous advantages compared with traditional methods, these have not found success because of their cost, their lack of reliability and their compatibility issues with standard materials and procedures. These harvesting systems have nevertheless paved the way for new methods of automating crystal harvesting and preparation for X-ray diffraction.

In this manuscript, we present the new Robotic Equipment for Automated Crystal Harvesting (REACH) recently developed on beamline FIP-BM30A at the European Synchrotron Radiation Facility (ESRF) in order to achieve more robust and reliable macromolecular crystal harvesting and flash-cooling operations that are compatible with most standard macromolecular crystallography equipment such as sitting-drop crystallization microplates.

2. Methods and materials

2.1. Samples

The 14.4 kDa lysozyme protein from hen egg white (Roche, catalogue No. 10837059001) was crystallized by mixing 500 nl of a 50 mg ml^{-1} protein solution in 0.24%(*w*/*w*) acetic acid with 500 nl 5%(*w*/*v*) NaCl reservoir solution. The 56.3 kDa NikA protein from *Escherichia coli* was also used. Its cytoplasmic apo form was expressed and purified as described previously by Cherrier *et al.* (2008). A 10 mg ml^{-1} apo NikA solution was pre-incubated overnight at 277 K with two molar equivalents of FeEDTA and this protein–ligand complex was crystallized by mixing 0.5 µl of this solution with a reservoir solution consisting of 0.5 µl 0.1 *M* sodium acetate pH 4.7, 1.5–1.95 *M* ammonium sulfate (Cherrier *et al.*, 2005). Protein samples were crystallized on CrystalQuick X plates (Supplementary Fig. S2[1]), a vapour-diffusion sitting-drop microplate (Bingel-Erlenmeyer *et al.*, 2011). CrystalQuick X was developed by Greiner Bio-One and the FIP-BM30A group and has been commercialized by NatX-ray. This microplate is an SBS-standard 96-well plate with two flat wells for sitting drops per reservoir (Supplementary Fig. S1). The geometry of this plate provides better access to drops for crystal manipulation (Supplementary Fig. S2*b*). The wells are 1.3 mm deep in the CrystalQuick X plate, whereas the wells in other plates are 3–4 mm deep. The plates were filled manually. They were then screened for pairs of crystals grown in the same drop. For each pair, one of the two crystals was harvested, cryoprotected and flash-cooled manually using LithoLoops (Molecular Dimensions) and the other using the REACH system.

2.2. Beamline

Experiments were carried out on beamline FIP-BM30A (Roth *et al.*, 2002) at the ESRF. This beamline uses a bending magnet as a source and delivers a monochromatic beam with an intensity of 5×10^{11} photons $(0.3 \times 0.3\ \text{mm}^2)^{-1}\ \text{s}^{-1}$ and 2×10^{-4} energy resolution at 12.5 keV. In these experiments the beam size was defined at 0.2 × 0.2 mm. An ADSC Q315r CCD detector was used to record the diffraction frames. Two goniometers were available on the beamline: an MD2 with an on-axis microscope (Maatel) and the G-Rob system. For these experiments the G-Rob system was used as the goniometer and the MD2 on-axis microscope was used to define the spindle position and to visualize the samples for centring in the X-ray beam. For each sample, X-ray diffraction data were collected with 1° oscillation at 0.98 Å wavelength.

2.3. G-Rob: the robotized goniometer

The REACH system takes advantage of the accuracy of the G-Rob robot arm and its goniometer capability. G-Rob is a multi-task robotic system based on a six-axis robot arm (Stäubli) developed on beamline FIP-BM30A at the ESRF (Grenoble, France). G-Rob is sufficiently accurate to operate as a goniometer (Jacquamet *et al.*, 2009). This system has been commercially available since 2009 (NatX-ray). It is able to collect X-ray diffraction data with a sphere of confusion radius of better than 15 µm for cooled samples and capillaries. On G-Rob, two motorized translations are installed at the end of

[1] Supplementary material has been deposited in the IUCr electronic archive (Reference: TZ5012). Services for accessing this material are described at the back of the journal.

the robot arm to centre each sample on the sixth axis of the robot, which is used as the spindle axis. In the present experiments, this centring operation is performed only once when G-Rob holds its micro-gripper tool before the harvesting operation. In so doing, once the crystal is transferred to the spindle position it is already centred into the beam with a positioning error of less than 10 µm. Thus, X-ray diffraction data can be collected right away.

2.4. The micro-gripper

The robot tool is a key element of REACH. It equips the G-Rob robot arm with a specially designed micro-gripper for crystal handling in order to harvest samples from microplates, to perform cryoprotection and flash-cooling and to expose the samples to the X-ray beam (Fig. 1). This new tool for the G-Rob system was developed in order to achieve harvesting of crystals from their crystallization drop by grabbing them with a two-finger piezo-electric micro-gripping device (Agnus *et al.*, 2009). Each finger has two degrees of freedom controlled with a resolution of 1.0 µm and a reproducibility of 0.1 µm. By combining symmetrical translations of both piezo-electrical fingers, an opening-gap range from 0 to 500 µm is possible. This micro-gripping device was developed by Femto-ST (Besançon, France) and has now been commercialized (Percipio-Robotics). The ending elements that touch the crystals are fabricated separately from the two-finger micro-gripper (Fig. 2). These ending elements are composed of an epoxy-based polymer called SU-8 (Ling *et al.*, 2009). The geometry of the ending elements was designed with a concave shape at the extremity. They are 60 µm wide (considering the addition of the two jaws) and 30 µm thick. This geometry is a good compromise between efficient gripping of crystals and a reduction of the volume of SU-8 exposed to X-rays in order to minimize scattering (Fig. 2*b*). Thus, crystals are exposed to X-rays in the micro-gripper by the G-Rob robot arm for data collection. SU-8 produces a very low X-ray scattering background (data not shown). Compared with other common materials used for the fabrication of crystal-harvesting loops, SU-8 shows a background scattering on X-ray exposure between those of Kapton and nylon. Also, the elasticity of SU-8 combined with the reduced thickness of the ending elements provides sufficient flexibility to limit the stress on the crystals. Indeed, a sufficient gripping pressure on the crystal is assumed when a deformation of the jaws, say a 10 µm deformation, becomes visible. In this case, the force applied to the crystal by each jaw can be estimated as 35 µN.

2.5. The Visualization Bench

This setup is completed by a fully motorized Visualization Bench equipped with an inverted microscope (×48 magnification), a three-direction motorized microplate holder and local control software with a user-friendly graphical user interface (GUI; written in Tcl/Tk). This software displays the drop image and provides several functions for plate screening and crystal tracking. Therefore, the Visualization Bench is a standalone system that can be used independently of the crystal-harvesting application. When used for crystal harvesting, it is installed close to the robot arm and the software is upgraded to provide buttons for control of the motion of the robot. This 'mouse' control can also be switched to a 'joystick' control. To ensure better robustness against network failure during remote operations, the software will be rebuilt with a client–server architecture. The server software application will run in a semi-automated mode. During the harvesting step, a time-out limit will lead to the cancellation of harvesting and to automated sealing of the reservoir. Upon

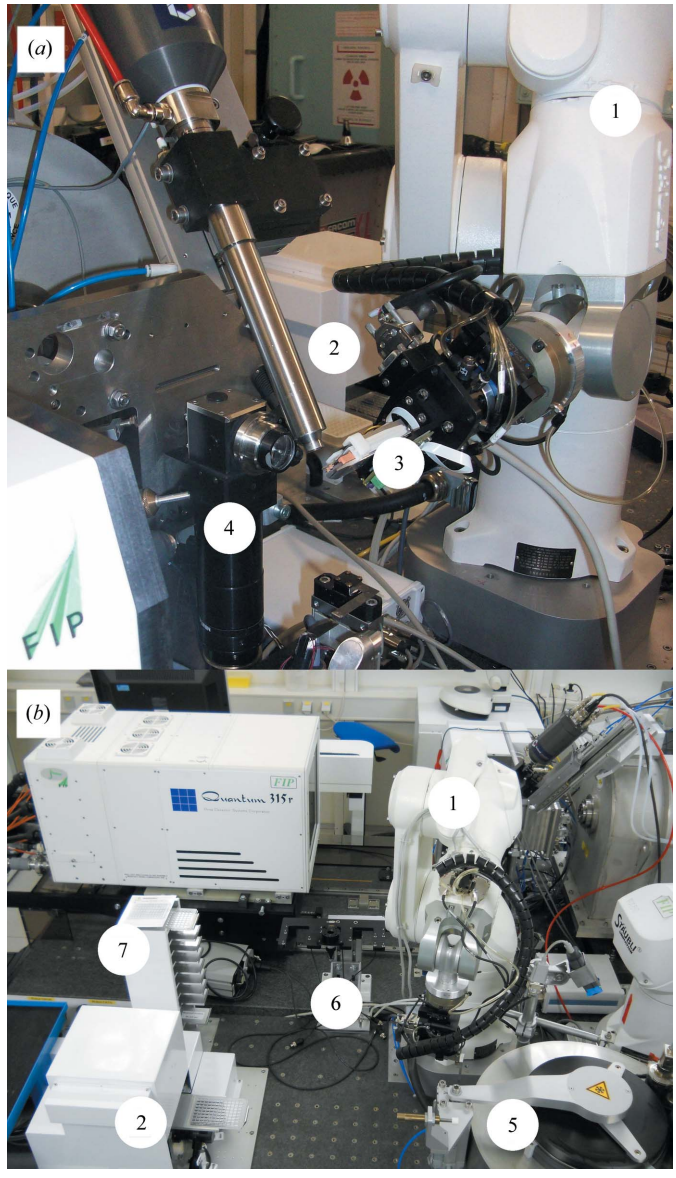

Figure 1
Experimental setup on the FIP-BM30A beamline. (*a*) Temporary setup used for the present work. The G-Rob robot arm (1), upon harvesting from the crystallization plates located on the Visualization Bench (2), presents the sample in the beam for data collection (3). The on-axis camera (4) is used for sample centring. (*b*) Setup under construction. Elements are rearranged for the robot arm (1) to reach access to the Visualization Bench for harvesting (2), the Dewar for storage of cooled samples (5), the robot tools magazine where the plate gripper, the micro-gripper and the goniometer head tools are stored (6) and the plate hotel (7).

crystal harvesting, no further communication with the client software will be required for the robot trajectory and the flash-cooling and reservoir-sealing steps.

Although the tests presented in this manuscript were made using the CrystalQuick X plate from Greiner Bio-One, the Visualization Bench is compatible with any SBS-format crystallization plate for sitting drops. Also, the ending elements of the micro-gripper are sufficiently long (5 mm) to harvest samples from deep drop wells.

2.6. Manual harvesting followed by data collection with G-Rob

In the manual method, the crystals were visualized using a classical laboratory binocular microscope and were harvested using SPINE-standard loops (Hampton Research, catalogue No. HR8-124). The crystals were then soaked in cryoprotecting solution [25%(*w*/*w*) glycerol and reservoir solution] for about 20–30 s and flash-cooled in a 100 K nitrogen-gas stream generated by a Cryostream 700 system (Oxford Cryosystems).

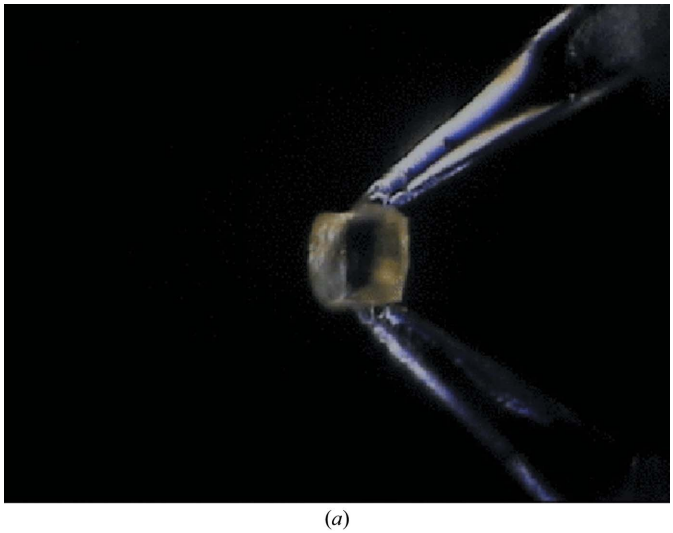

(*a*)

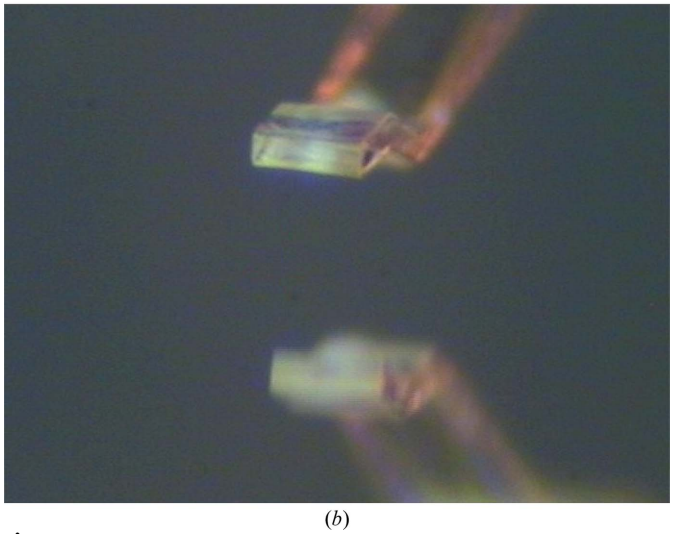

(*b*)

Figure 2
Image of the micro-gripper. (*a*) A lysozyme crystal handled by the micro-gripper. (*b*) Final generation of the ending elements, made of SU-8.

2.7. Using REACH followed by direct data collection with G-Rob

When using REACH, crystallization plates are screened using the Visualization Bench. Its GUI displays the microscope image. A drop of an appropriate cryoprotecting solution is dispensed over the crystallization drop. This could be a drop of oil that will ensure cyoprotection and limit evaporation at the same time. A button on the GUI sends the micro-gripper over the visualized well. Thus, control of the robot and micro-gripper is enabled through the GUI and a game pad. Thanks to the six-axis arm of G-Rob, the micro-gripper is capable of three translations and two rotational movements. Furthermore, control of the opening and closing of the micro-gripper is integrated into the GUI and into the game-pad buttons. Firstly, the motorized translations and zoom of the Visualization Bench are used to centre crystals in the microscope and to adjust the focus. The user then drives the movements of the G-Rob arm to approach the micro-gripper to crystals. The lighting is also controlled from the GUI to optimize vision quality. Once the crystal has been captured between the two SU-8 ending elements of the micro-gripper, a button on the GUI transfers the crystal with a safe but rapid trajectory into the nitrogen-gas stream to the spindle position. The trajectory of the robot during approach to the spindle position is programmed perpendicular to the 100 K stream with the robot's fastest speed to optimize flash-cooling. The trajectory ends at a position where the crystal is already centred on the spindle position. Since the G-Rob performs the goniometer task and the ending elements of the micro-gripper are transparent to X-rays, it was possible to proceed with data collection without releasing the crystal or any human manipulation.

2.8. Using REACH followed by transfer of the crystal on a loop

Alternatively, for sample storage, transfer of the harvested crystal on a loop was also tested. A manual goniometer head was placed in front of the Visualization Bench. An empty loop was plunged into a suitable cryoprotecting solution and was placed on the goniometer head. The HC1 system (Sanchez-Weatherby *et al.*, 2009) was used to blow a humidified room-temperature nitrogen stream onto the loop while harvesting and transferring the crystal to avoid dehydration. Once the crystal has been grabbed between the two ending elements of the micro-gripper, an automated robotic trajectory removes the crystal from its crystallization drop and transfers it to about 1 mm above the loop. A microscope and its light source were placed towards the loop in order to obtain a magnified view. The robot was then controlled with the game pad to release the crystal into the loop. Crystals were then cooled manually in liquid nitrogen

2.9. Diffraction data processing

Diffraction data were processed using *XDS* (Kabsch, 2010) and scaled with *SCALA* (Evans, 2006) from *CCP*4 (Winn *et al.*, 2011) or *XSCALE* from *XDS*. Phasing was performed by molecular replacement with *Phaser* (McCoy *et al.*, 2007) from

Table 1
Data and refinement statistics.

Comparison of data-set statistics for lysozyme and NikA–FeEDTA crystals harvested either manually ('Manual *X*') or with the REACH system ('Robotic *X*'). Values in parentheses are for the last shell.

	Lysozyme				NikA–FeEDTA			
Data set	Manual 1	Manual 2	Robotic 1	Robotic 2	Manual 1	Manual 2	Robotic 1	Robotic 2
Data collection								
Wavelength (Å)	0.97955	0.97955	0.9795	0.9797	0.97969	0.97968	0.97967	0.97967
Oscillation (°)	1	1	1	1	1	1	1	1
Rotation range (°)	60	90	69	110	75	110	90	90
Data reduction								
Space group	$P4_32_12$	$P4_32_12$	$P4_32_12$	$P4_32_12$	$P2_12_12_1$	$P2_12_12_1$	$P2_12_12_1$	$P2_12_12_1$
Resolution (Å)	38.65–1.50 (1.58–1.50)	36.78–1.80 (1.90–1.80)	38.62–1.75 (1.84–1.75)	38.99–1.60 (1.69–1.60)	47.01–2.65 (2.75–2.65)	40.70–1.85 (1.95–1.85)	44.25–2.30 (2.40–2.30)	44.22–1.95 (2.05–1.95)
Completeness (%)	84.7 (88.7)	100 (100)	99.9 (100)	99.7 (100)	97.4 (98.3)	97.9 (98.4)	98.6 (98.6)	97.3 (98.2)
Total reflections	84948 (11509)	73949 (10330)	59671 (8306)	125316 (16597)	90500 (9330)	380011 (54747)	163609 (19205)	267767 (37037)
Unique reflections	15560 (2324)	10887 (1548)	11761 (1671)	15436 (2201)	29023 (3015)	83913 (12171)	44557 (5294)	71555 (9924)
Multiplicity	5.5 (5.0)	6.8 (6.7)	5.1 (5.0)	8.1 (7.5)	3.1 (3.1)	4.5 (4.5)	3.7 (3.6)	3.7 (3.7)
$R_{\rm merge}$† (%)	4.9 (37.9)	5.5 (46.4)	8.8 (42.0)	5.8 (42.7)	12.4 (39.2)	4.7 (35.9)	5.6 (33.5)	5.3 (32.9)
$R_{\rm p.i.m.}$‡ (%)	2.2 (18.2)	2.3 (19.2)	4.3 (20.7)	2.2 (16.5)	8.7 (26.1)	2.6 (19.2)	3.7 (20.7)	3.5 (20.1)
$\langle I/\sigma(I)\rangle$	17.2 (3.9)	21.5 (4.1)	10.8 (4.5)	17.7 (3.8)	7.34 (2.92)	19.23 (4.40)	16.68 (4.35)	16.45 (4.51)
Mosaicity (°)	0.247	0.401	0.331	0.376	0.190	0.317	0.318	0.234
Unit-cell parameters (Å)	a = 77.31, b = 77.31, c = 36.97	a = 77.51, b = 77.51, c = 36.78	a = 77.30, b = 77.30, c = 36.89	a = 77.98, b = 77.98, c = 36.71	a = 86.28, b = 94.02, c = 123.3	a = 86.24, b = 93.64, c = 123.2	a = 86.24, b = 93.74, c = 123.4	a = 86.33, b = 93.88, c = 123.1
Refinement								
Resolution range (Å)	38.65–1.50 (1.59–1.50)	34.66–1.80 (1.89–1.80)	34.57–1.75 (1.84–1.75)	33.21–1.60 (1.65–1.60)	47.01–2.65 (2.74–2.65)	40.70–1.85 (1.87–1.85)	40.71–2.30 (2.35–2.30)	43.17–1.95 (1.98–1.95)
$R_{\rm work}$§ (%)	18.16 (22.45)	16.90 (21.34)	16.25 (20.00)	17.25 (21.72)	17.40 (22.95)	17.53 (27.20)	18.51 (25.34)	17.17 (25.63)
$R_{\rm free}$¶ (%)	20.21 (25.77)	21.61 (26.09)	19.74 (27.11)	19.37 (22.08)	26.91 (33.81)	21.55 (32.57)	25.47 (35.85)	21.65 (31.81)
R.m.s.d. bonds (Å)	0.006	0.007	0.008	0.008	0.008	0.007	0.008	0.008
R.m.s.d. angles (°)	1.063	1.062	1.187	1.125	1.150	1.124	1.087	1.117
Reflections in refinement	15534	10856	11725	15394	29015	83910	44550	71549
Average B factor (Å^2)	19.1	26.6	21.9	25.1	32.94	30.23	41.51	30.04

† $R_{\rm merge} = \sum_{hkl}\sum_i |I_i(hkl) - \langle I(hkl)\rangle|/\sum_{hkl}\sum_i I_i(hkl)$, where $I_i(hkl)$ is the intensity of a reflection and $\langle I(hkl)\rangle$ is the average intensity of that reflection. ‡ $R_{\rm p.i.m.} = \sum_{hkl}\{1/[N(hkl)-1]\}^{1/2}\sum_i |I_i(hkl) - \langle I(hkl)\rangle|/\sum_{hkl}\sum_i I_i(hkl)$, where N is the number of observations of the reflection. § $R_{\rm work} = \sum_{hkl} ||F_{\rm obs}| - |F_{\rm calc}||/\sum_{hkl}|F_{\rm obs}|$. ¶ $R_{\rm free}$ is the same as $R_{\rm work}$ but calculated for 5% data omitted from the refinement.

*CCP*4 using PDB entries 1lz8 (Dauter *et al.*, 1999) and 1zlq (Cherrier *et al.*, 2005) as starting models for lysozyme and NikA–FeEDTA, respectively. Refinement was performed using *PHENIX* (Adams *et al.*, 2010). Root-mean-square deviation (r.m.s.d.) values were calculated on main-chain atoms using *Coot* (Emsley & Cowtan, 2004).

3. Results

In order to assess the impact of the stress inflicted on crystals by the micro-gripper, a series of tests of harvesting and flash-cooling were conducted manually and with the REACH system (using the protocols described in §§2.6 and 2.7). In both cases, cryoprotection was achieved in the same way by the addition of a cryo-solution on top of the crystallization drop prior to harvesting, as described above. In the robotic method, crystals are directly exposed ('direct data collection') after being grabbed by the micro-gripper in order to evaluate the influence of gripping on crystal structure. Crystals of lysozyme and NikA–FeEDTA were used in this experiment (see §2). Two pairs of crystals from same wells of each protein were chosen and prepared for diffraction data collection with G-Rob using both manual and robotic methods.

Analysis of data reduction showed no significant differences in the mosaicity, resolution limits and unit-cell parameters (Table 1). Comparison of the unit-cell volumes of manually and robotically harvested samples (Table 2) also showed no significant differences. Nevertheless, their comparison with PDB entries 1zlq and 1lz8 for NikA–FeEDTA and lysozyme, respectively, showed variations of 1.4–3.6%. The diffraction data for lysozyme (PDB entry 1lz8) were collected at 120 K and not at 100 K. Thermal expansion cannot account for this difference. Indeed, calculations based on Tanaka (2001), considering the crystal and solvent as water, indicated only a 0.15% volume variation of each unit cell. Therefore, we assume that the unit-cell volume differences arise from the discrepancy in the experimental setup.

The data and refinement statistics were similar for crystals harvested using the robotic and manual methods. The r.m.s.d. values (Table 2) between the structures based on main-chain comparisons do not exceed 0.46 Å for both proteins. Thus, we can confirm that the stress on the crystals is controlled and that no structural rearrangement arises from use of the micro-gripper.

Although there was not a visible improvement in the data statistics, which was certainly a consequence of the reduced number of crystals tested, we observed a reduced amount of solvent around the crystal when harvesting with the robot. This resulted in reduced background scattering. The average background measured by *XDS* (INIT step) and normalized to

Table 2
Unit-cell changes between manually and robotically harvested crystals.

(*a*) Lysozyme.

	Comparative r.m.s.d. on main chain (Å)				Volume change (%)		
	1lz8	Manual 1	Manual 2	Robotic 1	Manual 1	Manual 2	Robotic 1
Manual 1	0.202	—	—	—	—	—	—
Manual 2	0.259	0.162	—	—	0.00	—	—
Robotic 1	0.223	0.083	0.123	—	0.24	0.24	—
Robotic 2	0.246	0.181	0.090	0.156	1.03	1.02	1.27

(*b*) NikA–FeEDTA.

	Comparative r.m.s.d. on main chain (Å)				Volume change (%)		
	1zlq	Manual 1	Manual 2	Robotic 1	Manual 1	Manual 2	Robotic 1
Manual 1	0.321	—	—	—	—	—	—
Manual 2	0.364	0.219	—	—	0.57	—	—
Robotic 1	0.470	0.289	0.210	—	0.24	0.33	—
Robotic 2	0.332	0.207	0.124	0.243	0.25	0.32	0.01

1 s exposure time and 1 mA current in the ESRF ring was 0.154 and 0.174, respectively, for lysozyme and NikA–FeEDTA when harvested manually. The average background was 0.126 and 0.071, respectively, when the crystals were harvested using the robot.

4. Discussion

4.1. Advantages of robotic harvesting

The use of REACH shows high accuracy and stability in manipulating crystals in their crystallization drops. In particular, this instrument significantly helps with the harvesting of crystals stuck to the bottom of crystallization plates. Indeed, with REACH crystals are gripped once and dragged without the need for repetitive contact. Crystals from 40 to 400 µm were manipulated and harvested successfully, even when grown in nanodrops in 96-well microplates. These tests revealed that harvesting very small crystals is significantly facilitated compared with manual harvesting. Apart from these difficult cases, the harvesting times for both manual and robotic methods were comparable. Rather, the time benefits for the REACH system arise from the subsequent steps. When using the robot, once harvested the crystal is already mounted on the G-Rob 'goniometer' and centred in the beam ready for data collection. Using the manual method, the sample holder has to be transferred to the goniometer head and the crystal-centring operation is mandatory as the loop dimensions and crystal position in the loop are random. This operation takes 1–2 min per crystal. Therefore, the robotic method provides higher reliability and repeatability, facilitates the harvesting of difficult crystals and saves time when coupled with direct data collection.

Also, the crystals harvested using REACH were transferred with a reduced amount of mother liquor and cryoprotecting solution compared with crystals harvested using a loop. A lower background owing to reduced diffusion rings was noticed with the robotic method in comparison with crystals harvested manually on a loop.

4.2. Film punching

To completely automate the procedure, the sealing film on the crystallization plate should be removed before crystal harvesting and resealed once the micro-gripper is out. An automated cutting system is under development to punch a portion of the sealing film using a heated wire. Experiments at room temperature show a maximum variation in the temperature of a 500 nl drop of less than 4 K after punching the sealing film with the heated wire that lasts for about 2 s. Sucking air smoothly around the heating wire with a small Venturi could avoid heat reaching the drop and could therefore diminish the temperature increase of the drop. At the end of the harvesting operation, an automated sealing device will stick a patch of tape over the hole to prevent evaporation and to save the drop.

4.3. Cryoprotection and flash-cooling with the micro-gripper

For the experiments presented above, cryoprotectant was added to the drop prior to harvesting. Alternatively, an automated procedure is being developed to soak the crystal using the micro-gripper into a cryoprotecting drop without releasing the crystal (Supplementary Fig. S1). The soaking time can be specified in the GUI, so that the robot will transfer the crystal to the spindle position automatically at the end of the soaking period. This procedure has been tested and the geometry of the ending elements has been improved to avoid releasing the crystal into the cryoprotecting drop (Fig. 2*b*). The quality of cooled crystals was not assessed by diffraction measurements.

4.4. Improved transfer to a loop

Initial attempts to transfer a crystal to a loop in a humidified gas stream after harvesting with the micro-gripper were performed but were not conclusive (§2.8; data not shown). In the future, a cryogenic stream will be used for rapid flash-cooling after transfer to the loop, instead of extended exposure to a humidified gas stream. The loop will be soaked in a cryoprotectant solution and held in a cryogenic stream. Two scenarios are considered: the loop will either be held by the goniometer or by the G-Rob goniometer head tool. Upon harvesting of the crystal by REACH, the cryogenic stream is suspended for the time necessary for transfer of the crystal from the micro-gripper to the loop. The cryogenic stream is then restored. The sample can then be exposed to X-rays or transferred to the storage Dewar.

5. Conclusion

A growing number of crystallization platforms are now coupled to beamlines. Also, a large number of core facilities, including both crystallization robots and an automated in-house X-ray source, are shared by several laboratories. In both cases, crystallization plates can be prepared locally and transferred directly to the X-ray setup, avoiding a damaging trip for crystallization drops. In such a context, methods for remotely controlled *in situ* screening experiments, as well as classical data collection from cooled crystals, are becoming easier. Our robotic harvesting method paves the way for fully remote-controlled protein crystallography experiments from crystallization assays to structure solution, as it provides the link between the two methods. The REACH system, complete with the tape-punching, sample-cryoprotection and flash-cooling steps described above, will provide such a complete high-throughput automated pipeline.

We thank the FIP-BM30A staff for their help with data collection. We would also like to thank Dr Richard Kahn (IBS, Grenoble), Dr Christine Cavazza (IBS), Dr Juan Sanchez-Weatherby (Diamond Light Source Ltd, Oxfordshire) and Dr Florence Pojer (EPFL, Lausanne) for help and support. We would also like to thank one of the anonymous reviewers for very detailed editing of the manuscript and for many helpful suggestions which have considerably improved the paper. The present project was funded by the Commissariat à l'Energie Atomique et aux Energies Alternatives (CEA), the Centre National de la Recherche Scientifique (CNRS) and NatX-ray. YH benefited from a PhD grant funded by CNRS and NatX-ray. The G-Rob system has been commercialized by NatX-ray (Saint Martin d'Hères, France) under a license agreement with CEA and CNRS. J-LF and XV are co-founders of NatX-ray. It is expected that the REACH system will also be commercialized by NatX-ray.

References

Adams, P. D. *et al.* (2010). *Acta Cryst.* D**66**, 213–221.
Adams, P. D. *et al.* (2011). *Methods*, **55**, 94–106.
Agnus, J., Hériban, D., Gauthier, M. & Pétrini, V. (2009). *Precis. Eng.* **33**, 542–548.
Bingel-Erlenmeyer, R., Olieric, V., Grimshaw, J. P. A., Gabadinho, J., Wang, X. & Ebner, S. G. (2011). *Cryst. Growth Des.* **11**, 916–923.
Cherrier, M. V., Cavazza, C., Bochot, C., Lemaire, D. & Fontecilla-Camps, J. C. (2008). *Biochemistry*, **47**, 9937–9943.
Cherrier, M. V., Martin, L., Cavazza, C., Jacquamet, L., Lemaire, D., Gaillard, J. & Fontecilla-Camps, J. C. (2005). *J. Am. Chem. Soc.* **127**, 10075–10082.
Cipriani, F., Röwer, M., Landret, C., Zander, U., Felisaz, F. & Márquez, J. A. (2012). *Acta Cryst.* D**68**, 1393–1399.
Dauter, Z., Dauter, M., de La Fortelle, E., Bricogne, G. & Sheldrick, G. M. (1999). *J. Mol. Biol.* **289**, 83–92.
Emsley, P. & Cowtan, K. (2004). *Acta Cryst.* D**60**, 2126–2132.
Evans, P. (2006). *Acta Cryst.* D**62**, 72–82.
Ferrer, J.-L. (2001). *Acta Cryst.* D**57**, 1752–1753.
Garman, E. F. & Schneider, T. R. (1997). *J. Appl. Cryst.* **30**, 211–237.
Georgiev, A., Allen, P. K. & Edstrom, W. (2004). *Proceedings of the IEEE/RSJ International Conference on Intelligent Robots and Systems (IROS 2004)*, Vol. 1, pp. 236–241. doi:10.1109/IROS.2004.1389358.
Georgiev, A., Vorobiev, S., Edstrom, W., Song, T., Laine, A., Hunt, J. & Allen, P. (2006). *Acta Cryst.* D**62**, 1039–1045.
Jacquamet, L., Joly, J., Bertoni, A., Charrault, P., Pirocchi, M., Vernede, X., Bouis, F., Borel, F., Périn, J.-P., Denis, T., Rechatin, J.-L. & Ferrer, J.-L. (2009). *J. Synchrotron Rad.* **16**, 14–21.
Jacquamet, L., Ohana, J., Joly, J., Borel, F., Pirocchi, M., Charrault, P., Bertoni, A., Israel-Gouy, P., Carpentier, P., Kozielski, F., Blot, D. & Ferrer, J.-L. (2004). *Structure*, **12**, 1219–1225.
Kabsch, W. (2010). *Acta Cryst.* D**66**, 125–132.
Kim, Y., Dementieva, I., Zhou, M., Wu, R., Lezondra, L., Quartey, P., Joachimiak, G., Korolev, O., Li, H. & Joachimiak, A. (2004). *J. Struct. Funct. Genomics*, **5**, 111–118.
Kriminski, S., Caylor, C. L., Nonato, M. C., Finkelstein, K. D. & Thorne, R. E. (2002). *Acta Cryst.* D**58**, 459–471.
Ling, Z., Liu, C. & Lian, K. (2009). *Microsyst. Technol.* **15**, 429–435.
Manjasetty, B. A., Turnbull, A. P., Panjikar, S., Büssow, K. & Chance, M. R. (2008). *Proteomics*, **8**, 612–625.
McCoy, A. J., Grosse-Kunstleve, R. W., Adams, P. D., Winn, M. D., Storoni, L. C. & Read, R. J. (2007). *J. Appl. Cryst.* **40**, 658–674.
McPherson, A. (1989). *Preparation and Analysis of Protein Crystals*. Malabar: Krieger.
Mueller-Dieckmann, J. (2006). *Acta Cryst.* D**62**, 1446–1452.
Ohara, K., Ohba, K., Tanikawa, T., Hiraki, M., Wakatsuki, S., Mizukawa, M. & Tanie, K. (2004). *Proceedings of the 2004 International Symposium on Micro-Nanomechatronics and Human Science*, pp. 301–306. doi:10.1109/MHS.2004.1421322.
Parkin, S. & Hope, H. (1998). *J. Appl. Cryst.* **31**, 945–953.
Roth, M., Carpentier, P., Kaïkati, O., Joly, J., Charrault, P., Pirocchi, M., Kahn, R., Fanchon, E., Jacquamet, L., Borel, F., Bertoni, A., Israel-Gouy, P. & Ferrer, J.-L. (2002). *Acta Cryst.* D**58**, 805–814.
Sanchez-Weatherby, J., Bowler, M. W., Huet, J., Gobbo, A., Felisaz, F., Lavault, B., Moya, R., Kadlec, J., Ravelli, R. B. G. & Cipriani, F. (2009). *Acta Cryst.* D**65**, 1237–1246.
Tanaka, H. (2001). *J. Mol. Liq.* **90**, 323–332.
Teng, T.-Y. (1990). *J. Appl. Cryst.* **23**, 387–391.
Viola, R., Walsh, J., Melka, A., Womack, W., Murphy, S., Riboldi-Tunnicliffe, A. & Rupp, B. (2011). *J. Struct. Funct. Genomics*, **12**, 77–82.
Warkentin, M., Berejnov, V., Husseini, N. S. & Thorne, R. E. (2006). *J. Appl. Cryst.* **39**, 805–811.
Winn, M. D. *et al.* (2011). *Acta Cryst.* D**67**, 235–242.